RESEARCH ARTICLE

Key Points:
- Results show semiannual peaks in mesospheric and E region echo occurrences with added annual peak in E region echo occurrence
- Mesospheric echo occurrence is governed by temperature inversion, wind shear, tidal, and gravity wave activities
- E region echo occurrence is governed by tidal and gravity wave activities

Correspondence to:
A. K. Patra,
akpatra@narl.gov.in

On the governing dynamics of the VHF radar echoes from the mesosphere and collision-dominated lower *E* region over Gadanki (13.5°N, 79.2°E)

D. Selvaraj[1] (iD), **A. K. Patra[2]** (iD), **S. Sathishkumar[3]**, **K. Kishore Kumar[4]**, and **D. Narayana Rao[1]**

[1]Department of Physics, SRM University, Chennai, India, [2]National Atmospheric Research Laboratory, Gadanki, India, [3]Equatorial Geophysical Research Laboratory, IIG, Tirunelveli, India, [4]Space Physics Laboratory, Vikram Sarabhai Space Centre, Trivandrum, India

Abstract In the present communication, the role of neutral dynamical processes in governing the morphology and seasonal variations of daytime VHF radar echoes from the mesosphere and the collision-dominated lower *E* region is discussed. While the seasonal variations of mesospheric echo occurrence show semiannual variation with their maxima in the equinoxes, the occurrence of *E* region echoes shows strong annual variation peaking in the summer with two secondary maxima identical to semiannual variation of the mesospheric echoes. The occurrence rates of the *E* region echoes, however, display year-to-year variability. Semiannual variations in the occurrence of low-latitude mesospheric echoes are closely linked with similar variations in the occurrences of temperature inversion, large wind shear, tides, and gravity wave activities in the same height region. In the case of *E* region echoes, the summer maximum and equinoctial secondary maxima are found to be linked with similar variations in wind and wind shear, E_s activity, tidal, and gravity wave activities. Further, the summer maximum is found to be strongly correlated with that of meteor flux and nonmigrating diurnal tide. This finding is significant given the fact that such wind field in the presence of metallic ions could form both E_s and field-aligned irregularities. The present results show that tides and gravity waves are the most important dynamical factors governing the morphology and seasonal variations of the mesospheric as well as lower *E* region echoes observed over Gadanki. These results are discussed in the light of current understanding on the dynamical coupling of the mesosphere and lower *E* region through tides and gravity waves.

1. Introduction

Very high frequency (VHF) radar echoes from the low-latitude mesosphere have been studied only from two locations in the world: Jicamarca (11.95°S, 76.87°W; magnetic latitude 0.2°S) in Peru and Gadanki (13.5°N, 79.2°E; magnetic latitude 6.5°N) in India [e.g., *Woodman and Guillen*, 1974; *Sasi and Vijayan*, 2001]. Simultaneous observations made using rocket-borne experiments and radar have clearly revealed that the mesospheric echoes are linked with electron density fluctuations generated by neutral turbulence [e.g., *Royrvik and Smith*, 1984; *Chandra et al.*, 2008]. Turbulence is generated either by convective or dynamical instability depending on the background temperature and wind fields. Radar observations have also revealed that the low-latitude mesospheric echoes could be linked with turbulent layer and/or spatially confined patchy regions [e.g., *Royrvik*, 1983; *Sheth et al.*, 2006; *Lehmacher et al.*, 2007; *Chandra et al.*, 2008; *Belova et al.*, 2012]. The descending layer-type morphology of the echoing regions, which indicate the potential role of tidal/gravity wave dynamics on the echoing morphology, however, have not been paid attention so far.

On the other hand, tidal/gravity wave imprints have been clearly noted in the radar observations of field-aligned irregularities (FAIs) from the low-latitude *E* region outside the electrojet belt [e.g., *Chau et al.*, 2002; *Patra et al.*, 2006; *Venkateswara Rao et al.*, 2008]. The *E* region FAIs observed at Gadanki have been found to be mostly governed by neutral wind and sporadic *E* layer (E_s) [e.g., *Patra et al.*, 2009], unlike those of the equatorial electrojet where the underlying strong current drives plasma irregularities. It has also been observed at Gadanki that much of the daytime *E* region FAI are confined to altitudes below 100 km [*Patra et al.*, 2004], where plasma is closely coupled with the neutral through ion-neutral collision.

Although we know that neutral dynamics plays an important role in providing free energy for both neutral turbulence and plasma instability generating electron density irregularities in the off-electrojet (outside the magnetic latitude belt of ±3°) low-latitude mesosphere and *E* region, it is not known what are the prime
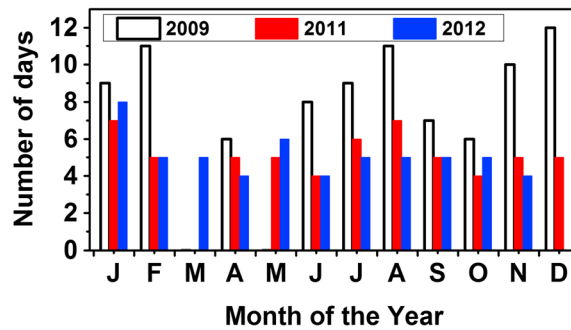
Figure 1. Distribution of number of days of MST radar observations used for the present study.

dynamical entities that govern the morphology and seasonal behavior of the mesospheric and E region echoes and what are the coupling processes involved in the two neighboring regions. In the present study, we attempt to identify the most important dynamical factors and their mutual dynamical coupling governing the morphologies and seasonalities of the low-latitude mesospheric and E region echoes.

2. Observational Data

For the present study, we use Gadanki mesosphere-stratosphere-troposphere (MST) radar observations of the mesospheric and E region echoes, Sounding of the Atmosphere using Broadband Emission Radiometry (SABER) and lidar observations of temperature, ionosonde observations of sporadic E layer parameters, MST and medium-frequency (MF) radar observations of wind, and meteor radar observations of meteor flux.

Observations of mesospheric and ionospheric E region echoes used in the present study were made in 2011 and 2012 using the Gadanki MST radar [*Rao et al.*, 1995]. These observations were made during daytime (9:30–16:00 Indian Standard Time = UT + 5.5 h). Observations were made using three noncoplanar beam directions: vertical, 14° off zenith due east (hereafter E-14°), and 14° off zenith due north (hereafter N-14°) so that echo characteristics and winds in the mesosphere and E region FAI can be studied. It may be mentioned that over Gadanki, the E region FAIs are observed when the radar beam is pointed at 14° off zenith due north to be perpendicular to Earth's magnetic field ($\mathbf{k} \perp \mathbf{B}$ condition, where $\mathbf{k}$ is the wave vector of the radar and $\mathbf{B}$ is the Earth's magnetic field). Radar observations were made in the form of Doppler power spectrum with a range resolution of 1.2 km (corresponding to a pulse width of 8 μs) and time resolution of 50 s. Details on these observations and spectral parameter estimation can be found in *Selvaraj et al.* [2016]. In addition to these, we have used simultaneous observations of E region FAI and ionosonde observations of E_s made in 2009 to study the relationship between them. We have used the 2009 observations since E_s observations were not made in 2011 and 2012 due to technical problems of the ionosonde. Figure 1 shows monthly distributions of data used in the present study. Monthly distributions of number of observational days in 2011 and 2012 are shown by red and blue bars, respectively, while those made in 2009 are shown by unfilled bars. Note that no observation was made in March and May 2009, March 2011, and December 2012.

E layer characteristics have been studied using observations made in 2009 by a collocated ionosonde [*Patra et al.*, 2012]. Importantly, in the present study we have paid special attention to distinguish E_s layer from E layer and observations related to E_s have been used for comparison with the radar observations of FAI. We noted that the E layer peak frequency follows solar zenith angle dependence and accordingly displays local time variations. Observations having peak frequencies in excess of E layer peak frequency have been considered as E_s. Here we use height and blanketing frequency of the E_s layer (fbE_s) to study linkage between the E region FAI and E_s layer properties.

Daytime mesospheric temperature observations used here have been taken from the SABER database (http://saber.gats-inc.com/). These observations facilitate us to construct seasonal variations and to examine the linkage between the mesospheric echoes and temperature field. They, however, do not provide local time variations required for studying tidal or gravity wave variations. For this purpose, we have used temperature observations made using a collocated Rayleigh lidar operating at a wavelength of 532 nm [e.g., *Siva Kumar et al.*, 2001]. Observations were made with a height resolution of 300 m and time resolution of 4.2 min. It may be mentioned that these observations were made during nighttime and hence are not directly applicable to interpret the daytime radar observations of mesospheric echoes. These, however, provide us height structure of temperature and their temporal variations.
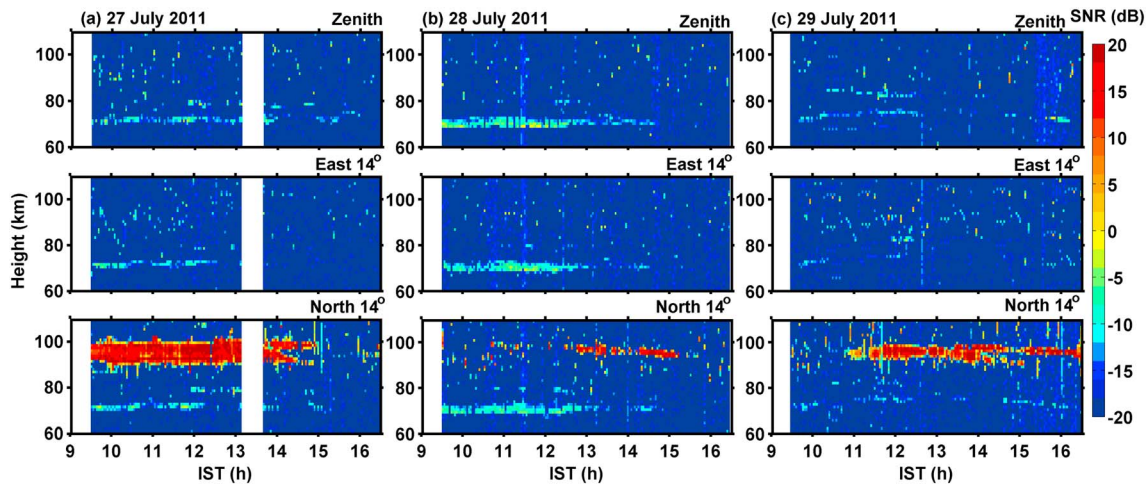
Figure 2. Height-time variations of SNR of radar echoes observed by the zenith beam (top), East-14° beam (middle), and North-14° beam (bottom) on (a) 27 July, (b) 28 July, and (c) 29 July 2011. White portions represent data gaps.

Observations on upper mesospheric winds used here were made using a MF radar, operating at 1.98 MHz, from Tirunelveli (8.7°N, 77.8°E) [*Rajaram and Gurubaran*, 1998]. It provides horizontal winds using spaced antenna technique in the height region of 80–98 km at every 2 km height interval and 2 min time interval. For the present study, we use hourly values of zonal and meridional winds.

Observations of meteor flux were made using a meteor radar, operating at 35.25 MHz, from Trivandrum (8.5°N, 77°E) [*Kumar et al.*, 2007a]. For the present purpose, we have used only the sporadic meteor flux.

3. Observational Results

3.1. Three-Beam Observations of Mesospheric and *E* Region Echoes

Figures 2a–2c show three examples of radar observations made on 27, 28, and 29 July 2011, respectively. In each figure the top to bottom panels show height-time variations of SNR of radar echoes observed by the zenith, East-14° and North-14° beams, respectively. It may be noted that the while the echoes occurring below 85 km were observed in all the three beams, the echoes occurring in the height range of 90–100 km were observed only in the N-14° beam, which satisfies perpendicularity to Earth's magnetic field. The echoes occurring in the height range of 90–100 km are linked with the FAI in the lower part of the *E* region and are generated by the gradient drift instability (GDI) process [*Patra et al.*, 2009].

3.2. Seasonal Variations of the Mesospheric and *E* Region Echoes

Figure 3 shows height-time distribution of echo occurrence in different seasons (top to bottom panels) for different beam positions (left to right panels). Occurrence rate has been calculated using echoes having signal-to-noise ratio (SNR) > -13 dB, and the height and time bins are 1.2 km and 3 min, respectively. These figures show that while the mesospheric echoes are observed in all the three beams, the *E* region echoes are observed only when the radar beam satisfies $\mathbf{k} \perp \mathbf{B}$ condition (i.e., in the N-14° beam). It may be noted that occurrence rates of the mesospheric echoes in the three beams are nearly similar. Echoing morphology and occurrence rates, however, vary considerably with season. For example, in the spring equinox, the mesospheric echoes occur in the form of two closely separated layers when compared to those in other seasons. On the other hand, occurrence rates of the mesospheric echoes are higher in the equinoxes (20%) than in the solstices (10%). For the *E* region echoes, except for the winter, occurrence rate is higher (as high as 30%) than those of the mesospheric echoes (10–20%). In the winter, occurrence rate of the *E* region echoes is generally low and is quite similar to that of the mesospheric echoes. A striking observation is that the occurrence rates of the *E* region echoes during the afternoon hours in both the equinoxes are lower than those in the forenoon. Also, the *E* region echoes are found to occur at higher altitudes in the fall equinox than in the spring equinox.
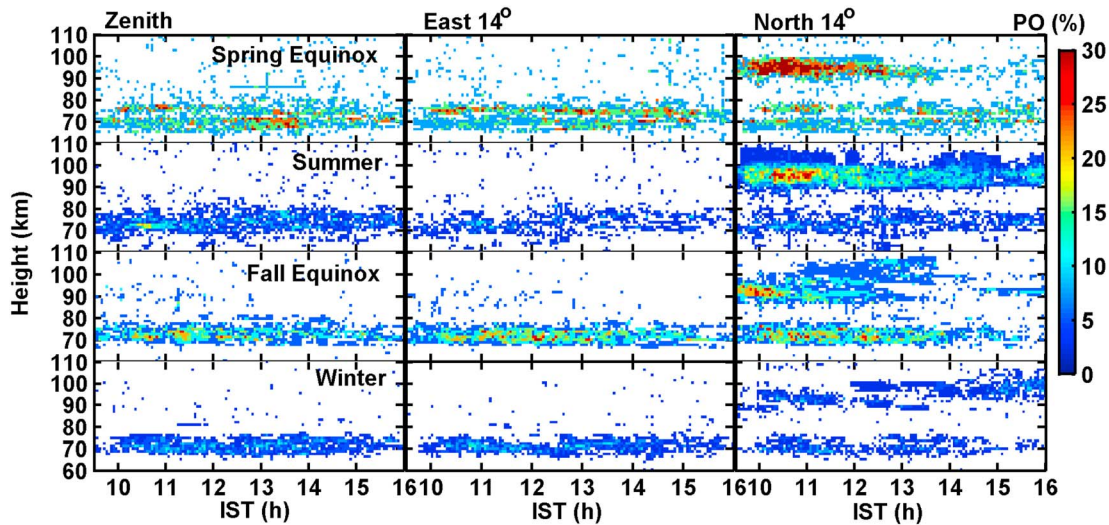
Figure 3. Height-time variations in the percentage occurrence of mesospheric and ionospheric *E* region echoes for winter, spring equinox, summer, and fall equinox observed in the zenith, East-14°, and North-14° beam directions.

Figure 4 provides an overall view on the seasonal variations of the mesospheric and *E* region echo occurrence. This figure presents height profile of monthly occurrence rate of echoes estimated using radar observations made in 2011 and 2012. Also, since the *E* region echoes are observed only in the N-14° beam, occurrence rates in the height region of 60–83 km have been computed using observations made using the three beams, while in the height region above 83 km occurrence rates have been computed based on observations made by the N-14° beam only. Figure 4 clearly shows that the mesospheric and *E* region echoes mostly occur in the height ranges of 65–77 km and 87–102 km, respectively. Both echoing phenomena show remarkable seasonal variations. Occurrence rate of the mesospheric echoes maximizes in the equinoxes, consistent with the results reported earlier from Gadanki [*Kumar et al.*, 2007b]. In the spring equinox, the mesospheric echoes occur in distinctly separate height regions unlike in the fall equinox. Occurrence rate of the *E* region echoes maximizes in the summer with secondary maxima in the equinoxes and minimum in the winter. The equinoctial secondary maxima, however, should be viewed with care given the fact that the *E* region echoes occur very less in the afternoon of both equinoxes. After accounting for this detailed occurrence patterns, we find that the mesospheric and *E* region echoes has some common seasonal features: they occur more in the equinoxes and summer than in the winter. Occurrence rate of the *E* region echoes, however, is overwhelmed in the summer when compared to the mesospheric echoes.
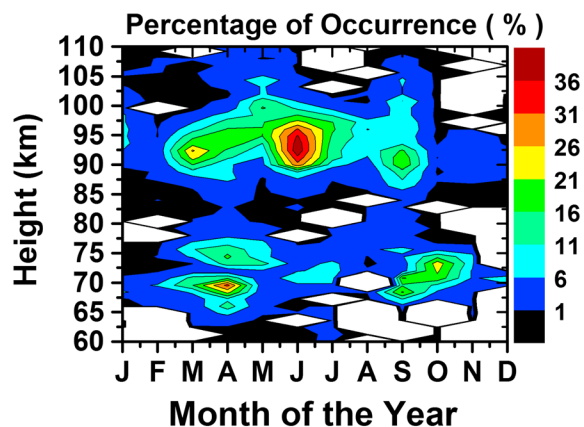

Figure 4. Seasonal variations of percentage occurrence of mesospheric and ionospheric *E* region echoes observed during 2011–2012.
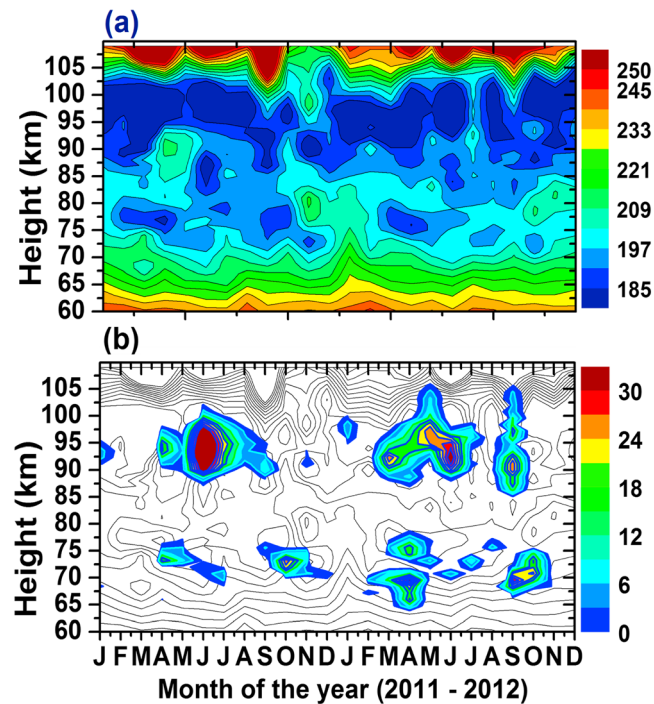
Figure 5. (a) Seasonal variations of mesospheric temperature obtained from SABER during 2011–2012. (b) Seasonal variations of percentage occurrence of mesospheric and ionospheric *E* region echoes overplotted on temperature.

3.3. Relationship Between Echoing Regions and Thermal Structure

In order to gain some insight on the possible relationship between the echoing region and thermal structure at these altitudes, we have examined temperature observations from the SABER made in 2011 and 2012. Figure 5a shows monthly mean temperature variations over Gadanki (in a latitude-longitude grid of $10° \times 10°$). This figure clearly shows minimum temperature occurring around 98 km with a secondary minimum occurring around 77 km. The secondary minimum, however, either did not occur or less pronounced in winter. The observed thermal structure has both seasonal and interannual variability. Intriguingly, the secondary minimum shows descending pattern, with a descent rate of ~1 km/month, occurring twice a year. These descending patterns, however, are clearer in 2011 than in 2012.

In Figure 5b, we overlay the occurrence map of radar echoes on the temperature map shown in Figure 5a. Temperature observations have been redrawn in the form of black contours, and occurrence rates of echoes are shown in color so as to correlate the echoing regions and the background temperature field. As is evident, the mesospheric echoes are collocated with the negative temperature gradients associated with the secondary temperature minima. It is interesting to note that the mesospheric echoing regions also display descending patterns quite similar to those in the temperature structures. Again, the descending patterns in the mesospheric echoes are found to be clearer in 2011 than in 2012. Notwithstanding the variations in the temperature field and the occurrence rate of the mesospheric echoes observed in 2011 and 2012, the observed correlation between the temperature gradient and echo occurrence assumes importance given the fact that negative temperature gradient could provide conducive condition for setting in instability. It is intriguing to note that the mesospheric echoes are absent where temperature gradient is minimum. Case studies based on radar observations and concurrent temperature observations from the SABER (not presented), however, suggest that while mesospheric echoes were found to be generally associated with regions of enhanced negative temperature gradient, all regions with enhanced negative temperature gradient did not accompany mesospheric echoes. Later, we will examine the other free energy sources responsible for the mesospheric echoes.

Coming to the *E* region echoes, they are found to occur in the mesopause region (a region of the lowest temperature). Considering that they are field aligned (Figure 2) and are linked with the *E* region plasma instability processes, their occurrence in the mesopause is primarily a happenstance. While there may be some effect of
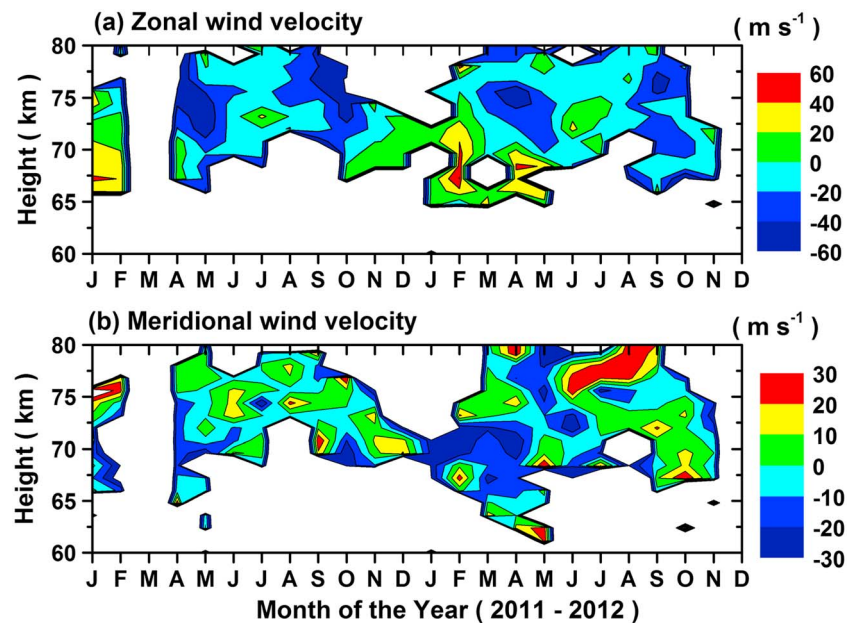
Figure 6. Seasonal variations of mesospheric (a) zonal and (b) meridional winds observed using the MST radar.

the low temperature in the instability process through the collision frequency, the primary source of free energy lies in the electron density gradient, presumably linked with E_s layer, and zonal wind. Thus, we will examine the roles of sporadic E layer and zonal wind for their occurrence.

3.4. Role of Wind and Wind Shear

Wind and wind shears are important free energy sources for setting in neutral and plasma instabilities. In the mesosphere, wind shear can provide condition for Kelvin-Helmholtz instability. In the lower E region, zonal wind shear can form E_s layer (through ion convergence), providing sharp density gradient, which can become unstable through the GDI. The same zonal wind also can either enhance or decrease the differential motion between the electrons and ions, which is an important factor for the growth of the GDI. For this purpose, we have examined the MST radar observed winds in the lower mesosphere and MF radar observed winds in the upper mesosphere.

Figures 6a and 6b show the monthly mean zonal and meridional components of wind, respectively, obtained using the MST radar observations of mesospheric echoes made in 2011 and 2012. Note the data gaps in March 2011 and December 2012. Additional data gaps are due to nonoccurrence of the mesospheric echoes. Zonal and meridional components of wind are in the range of $\pm 60\,\mathrm{m\,s^{-1}}$ and $\pm 30\,\mathrm{m\,s^{-1}}$, respectively. Note the presence of large westward winds at around 75 km in both equinoxes of 2011 and 2012, signifying mesospheric semiannual oscillation. Also note that there exists considerable wind shear both at the bottom and the top of the westward wind regime. During the rest of the period, such large wind and wind shear were not present. It is apparent from Figures 5 and 6 that in the equinoxes, there is a reasonably good correlation between the echo occurrence rate and large wind and wind shear as well as the negative temperature gradient associated with temperature inversion.

Figures 7a and 7b show zonal wind observed using the MF radar from Tirunelveli. We consider only zonal wind since it is relevant for understanding the formation of E_s and E region FAI. Figure 7a shows monthly mean zonal wind in the height region of 80–98 km. Note that the zonal winds in every month display vertical shear: zonal wind is eastward (or small westward) at lower heights and westward (or large westward) at higher heights. It is important to note that zonal wind is eastward at lower height in May–July when the E region FAI occurred maximum. As mentioned before, such wind system is conducive for E_s formation via the wind shear mechanism, and also, the eastward wind enhances the differential motion between the electrons and ions, which are important for generating FAI. It is also important to note that zonal winds during
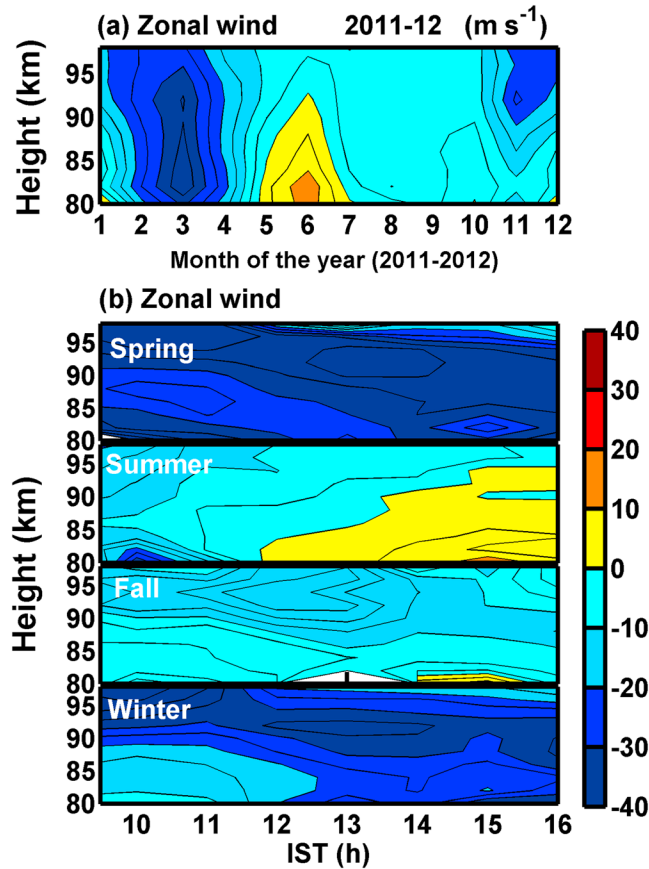
Figure 7. (a) Seasonal variations of zonal win in the upper mesosphere and (b) height-time variation of zonal wind in the upper mesosphere in different seasons measured using Tirunelveli MF radar.

April–September are either less westward or eastward at lower heights, which are found to be quite consistent with the occurrence pattern of FAI.

Figure 7b shows height profile of zonal wind with local time in different seasons. Note that the seasonal mean winds are either eastward or small westward at lower altitudes and with increasing height they become westward or large westward. Importantly, note that except in the summer the wind system shows a descending phase of wind gradient (small westward at lower altitudes and large westward at higher altitudes) consistent with tidal behavior. In the summer also while wind shear can be noticed, the wind pattern is very different. Later we will discuss the tidal features further.

3.5. Role of Sporadic E Layer

Since E_s observations are not available for 2011 and 2012, we have used observations of FAI and E_s made in 2009 to evaluate the role of E_s in forming FAI. We have also used observations of upper mesospheric wind made from Tirunelveli to examine the consistency between E_s and zonal wind shear. Figures 8a and 8b show seasonal variations in the occurrence of FAI and occurrence (red) and blanketing frequency (blue) of E_s, respectively. Figure 8c shows zonal wind for the fall equinox and winter (observations during spring equinox and summer were not made). Figure 8a clearly shows that the overall occurrence of the E region FAI in 2009 is high in the summer, moderate in the equinoxes, and minimum in the winter. In addition, in the equinoxes, occurrence of the FAI is higher in the forenoon than in the afternoon. The echo occurrence rate in 2009, however, is higher than that during 2011–2012, and also, the occurrence rate of the E region FAI in the forenoon of spring equinox is higher than those of other seasons. Except for these detailed differences, we find that the overall occurrence patterns of the E region FAI are broadly similar to those of 2011–2012. Figure 8b shows occurrence of E_s (in red) and median fbE_s (in blue) in different seasons. In general, occurrence of E_s is found to be maximum in the summer, moderate in the equinoxes, and minimum in the winter. The median values of fbE_s also follow similar seasonal variations. Notably, both E_s occurrence and fbE_s are very small in the winter. These observations clearly suggest a close coupling between E region FAI and E_s (both occurrence and fbE_s).

In the case of zonal wind (Figure 8c), we find that vertical shear exists both in the fall equinox and winter in the form of eastward wind at lower altitudes and westward wind at higher altitudes. Also, the height of reversal in zonal wind and its local time variations are reminiscent of descending tidal node. The westward wind, however, is stronger in the winter than in the fall equinox, and this difference appears to be responsible for lower occurrence rates of FAI and E_s (including fbE_s) in the winter than in the fall equinox. It is also important to note that zonal wind in 2009 is predominantly eastward at lower altitudes and small westward at higher altitudes when compared to small westward wind at lower altitudes and large westward wind at higher altitudes in 2011–2012. Assuming that zonal wind is important for the formation of E_s and FAI, the difference in
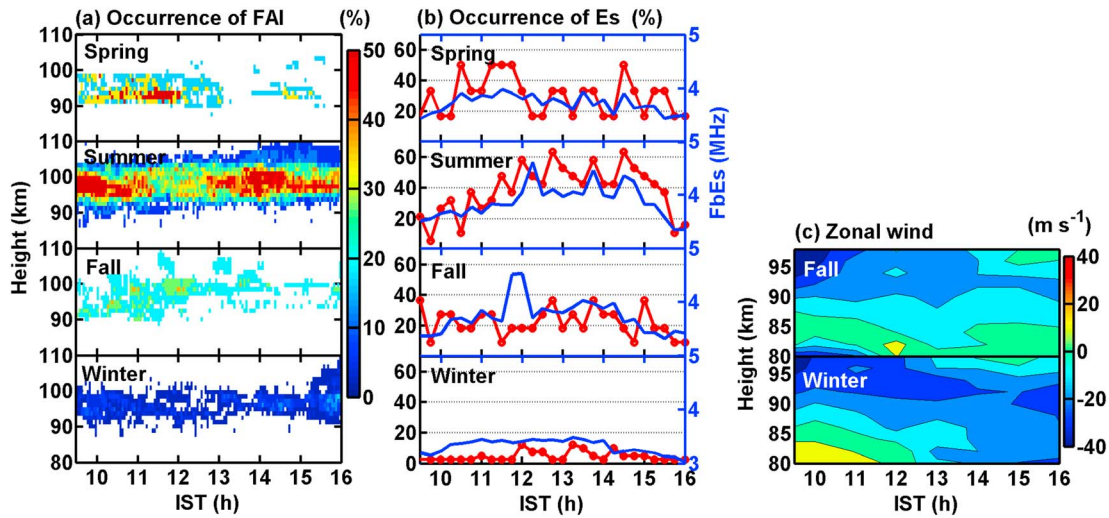
Figure 8. (a) Height-time variations of percentage occurrence of mesospheric and *E* region echoes in different seasons in 2009 observed by MST radar. (b) Local time variations of percentage occurrence of sporadic *E* (red lines) and fb*E*$_s$ (blue lines) in different seasons in 2009 observed using a collocated ionosonde. (c) Height-time variations of zonal wind observed in the fall equinox and winter in 2009 using the Tirunelveli MF radar.

the wind system in 2009 and 2011–2012 also appears to be consistent with the overall higher occurrence rate of *E* region FAI in 2009 than in 2011–2012. Unfortunately, we do not have *E*$_s$ observations during 2011–2012 to compare the *E*$_s$ properties with zonal wind shear and the *E* region FAI.

3.6. Role of Metallic Ions

Since metallic ions are the important ingredients of the *E*$_s$ and metallic ions are of meteoric origin, we have examined observations of meteor count. Figure 9 shows daily variations of meteor count (a proxy of metallic ion input) observed in 2011 (blue) and 2012 (red) using a meteor wind radar located at Trivandrum. The black line represents the average of the 2011 and 2012 observations. Meteor count is found to maximize in the summer, moderate in the winter, and minimum during the equinoxes. Large meteor flux and wind system observed during May–August appear to be quite consistent with the occurrence of the *E* region FAI. In the equinoxes and winter, however, such a clear corroboration is not seen. For example, meteor count is high and wind system is more conducive in the winter than in the spring equinox, but the occurrence of the *E* region FAI is lower in the winter than in the spring equinox. This observation is a bit puzzling. The seasonal variations in the occurrence of the *E* region FAI, however, are broadly consistent with the *E*$_s$ seasonality observed in 2009. Due to lack of *E*$_s$ observations in 2011 and 2012, we are unable to make a one-to-one comparison of zonal wind, *E*$_s$ and *E* region FAI, a task to be taken up in a future study.
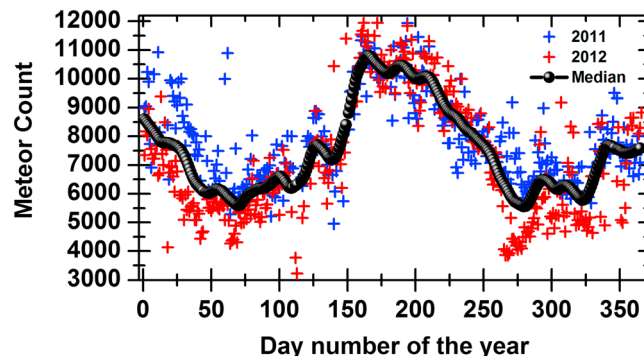

Figure 9. Seasonal variations of meteor flux observed in 2011 (in blue) and 2012 (in red) using the meteor radar at Trivandrum. Black circles represent the average of 2011 and 2012 observations.
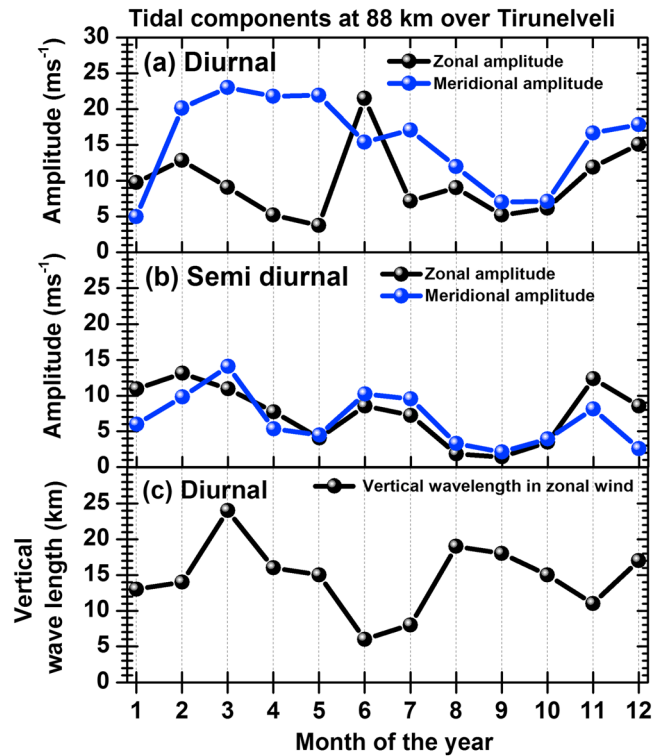
Figure 10. (a and b) Seasonal variations of diurnal and semidiurnal tidal amplitudes in zonal and meridional winds at 88 km derived using MF radar observations. (c) Seasonal variations in the vertical wavelength of diurnal tide.

3.7. Role of Tides

In an attempt to comprehend the plausible role of tides on the seasonal variations of the mesospheric and *E* region echoes, we have examined seasonal variations in the diurnal and semidiurnal tidal characteristics derived using MF radar measured winds. Figures 10a and 10b show diurnal and semidiurnal tidal amplitudes at 88 km, respectively. The black (blue) lines represent diurnal and semidiurnal tidal amplitudes in zonal (meridional) wind. The diurnal tidal amplitude in the meridional wind is generally stronger than that in zonal wind except for June. The seasonal variation in this, however, is not similar to the mesospheric and *E* region FAI occurrence. In contrast, the seasonal variations in diurnal tidal amplitude in the zonal wind have a good correspondence with those of the mesospheric and *E* region FAI occurrence. In June the diurnal tidal amplitude in the zonal wind is remarkably higher than those in other months consistent with the FAI occurrence. Semidiurnal tidal amplitudes are more or less similar and have similar seasonal variations: they have three peaks occurring in the two equinoxes and summer. Their seasonal variations have a close correspondence with the *E* region FAI occurrence. The peaks in the diurnal tidal amplitudes, however, occur slightly before the spring equinox and after the fall equinox. Thus, barring some difference, the seasonal variations in the tidal amplitudes in the zonal wind and the *E* region FAI appear to be quite similar. The lack of one-to-one correspondence between tidal amplitude and the *E* region FAI occurrence in the equinoxes could partly be due to the fact that the winds correspond to 88 km (10 km lower than those of the *E* region FAI) and 8.5°N latitude (5° lower latitude than that of Gadanki). The semidiurnal tides, however, have large vertical wavelengths, and hence, the zonal wind shears associated with those are not very efficient in the ion convergence at the lower *E* region. Thus, in the following we discuss on the vertical wavelength of diurnal tide in an effort to understand the close linkage between the diurnal tidal amplitude and FAI occurrence.

Figure 10c shows seasonal variations of vertical wavelength of diurnal tide in zonal wind. It is interesting to note that the vertical wavelength of diurnal tide is ~7 km in June and July when compared to 10–25 km in other months. We surmise that the diurnal tide with large amplitude and short vertical wavelength in June is nonmigrating consistent with the results reported by *Sridharan and Sandhya* [2014]. The short vertical wavelength suggests low downward phase progression, and hence, the tidal forcing can be effective for long
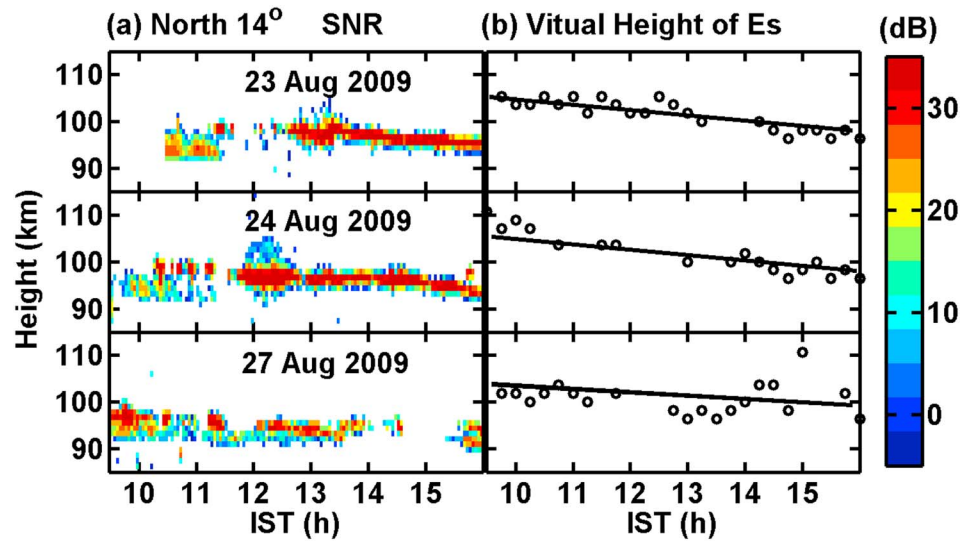
Figure 11. (a) Height-time variations in SNR of ionospheric E region echoes observed using North-14° beam directions on different days. (b) Time variation of height of the E_s layer on different days.

period in converging ions forming E_s layer. Taking the vertical wavelength as 7 km, the phase progression is estimated to be ~0.3 km/h, implying that the wind system of such tidal behavior would move only 3.5 km during the entire day. This wind system will be very effective in forming and sustaining E_s layer. This finding is consistent with the daylong observations of FAI with large occurrence rate in the summer. In contrast, in the equinoctial months, the vertical wavelength being close to 20 km, the E_s layer formed by such wind would move 10 km (about 1 km/h) during the daylight hours. This implies that when the E_s layer moves downward by 10 km, the layer would not be suitable for plasma instability due to recombination of ions at lower altitudes. The observed tidal wind field suggests that the node moves to the collision-dominated lower E region in the afternoon and dump all the metallic ions in the form of neutral metal. This qualitatively explains the forenoon-afternoon asymmetry in the FAI occurrence in the equinoxes.
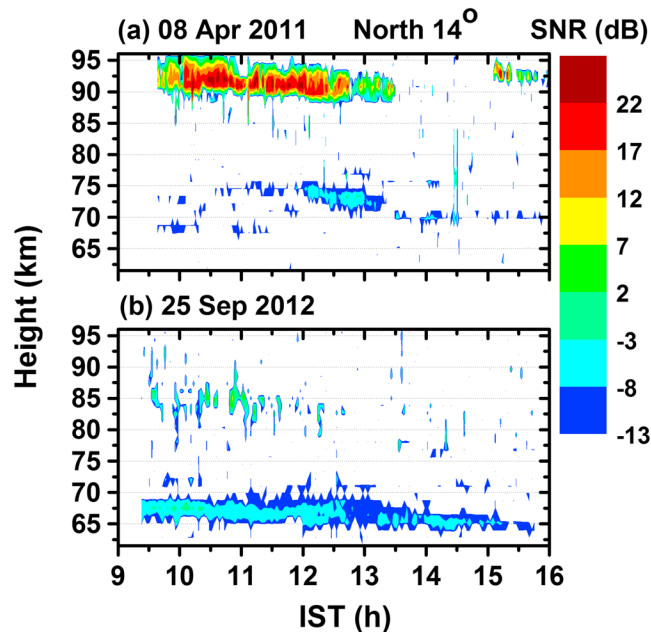
Figure 11 shows height-time variations of SNR of the E region echoes (Figure 11a) and corresponding variations in the E_s virtual height (Figure 11b), observed on 23, 24, and 27 August 2009, to demonstrate the descending properties of the E region FAI and E_s. Both show descending patterns with a descent rate of ~1 km/h, which is consistent with migrating diurnal tide. It may be recalled from Figures 7, 8 that zonal wind field also has vertical shear and the descent rate of the shear node is consistent with the diurnal tidal characteristics. Considering that the E region FAI can be generated on the electron density gradients associated with E_s layer, the observed close correlation
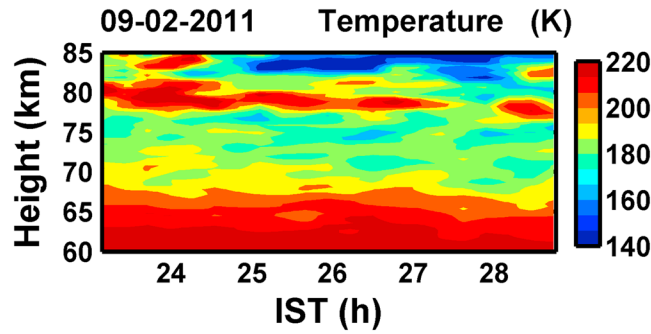

Figure 12. Height-time variation of SNR of mesospheric and E region echoes observed on (a) 25 April 2011 and (b) 25 September 2012 in the N-14° beam direction.

Figure 13. Height-time variation of mesospheric temperature displaying tidal signature measured using Rayleigh lidar on 9 February 2011.

between the E_s and E region FAI clearly suggests the role of tidal wind in governing the E_s and FAI.

Figures 12a and 12b show height-time variations of SNR of the mesospheric echoes observed using the North-14° beam on 8 April 2011 and 25 September 2012, respectively. Observations made using the N-14° beam have been chosen to illustrate both mesospheric and E region echoes. In both examples, the height of the mesospheric echoes is found to decrease with time. Similar descent has also been noted in the mesospheric echoes observed in the vertical beam (not shown). Coming to the E region echoes, they also display similar descending features. On 25 September, however, the E region echoes were observed at lower heights than those observed on 8 April and the echoes did not occur continuously. The fact that these echoes were not observed in the vertical beam implies that they are FAI but occurring at unusually low altitudes. Such low-altitude FAI echoes have seldom been observed at Gadanki [*Patra et al.*, 2006]. It is important to note that the descent rates of the mesospheric and E region echoing layers are ~1 km/h and these two echoing layers are separated by about 20 km, which are quite consistent with the characteristics of diurnal tide.

To demonstrate the tidal signature in temperature, in Figure 13 we present height-time variations of temperature estimated using lidar observations made from Gadanki on 9 February 2011. Note that the mesospheric temperature inversion occurred in between 75 km and 80 km. The most striking result is the slow descent of the temperature inversion region. The descent rate of the temperature inversion region is estimated to be ~1 km/h. The descent rate of ~1 km/h is very similar to the descent rate of the mesospheric echoing layer shown in Figure 12 and is consistent with that expected from diurnal tide. While the role of diurnal tide on the temperature inversion layer is quite evident in this example, further investigation is required using a larger database of long-duration lidar observations.

3.8. Role of Gravity Waves

To study the role of gravity waves, in Figure 14 we reproduce the seasonal variations of gravity wave-associated kinetic energy, E_k, reported earlier by *Selvaraj et al.* [2016] based on the MST radar observations of mesospheric winds made during 2011 and 2012. E_k has been estimated as $E_k = \rho(u'^2 + v'^2 + w'^2)$, where ρ is atmospheric density taken from the MSISE-90 model [*Hedin*, 1991] and $(u'^2 + v'^2 + w'^2)$ is wind variance associated with the gravity waves having periods in the range of 10 min to 4 h (for details, see *Selvaraj et al.* [2016]). The vertical bars represent 25 to 75 percen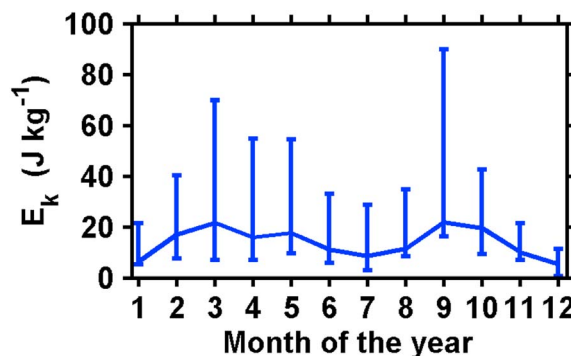tiles of variance for each month, estimated using daily observations of variance in the height region of 65–80 km. This figure clearly shows that gravity wave activities are maximum in the equinoxes and minimum in the summer and winter, consistent with the seasonal variations of echo occurrence. Similar seasonal variations in the gravity wave activity in the upper mesosphere (84–94 km) have also been reported before using the Tirunelveli MF radar observations [*Sridharan and Sathishkumar*, 2008].

Figure 14. Seasonal variation of gravity wave associated kinetic energy in the mesosphere estimated using MST radar observations of winds.

4. Summary and Discussion

Important results on the mesospheric and E region echoes and the governing background atmospheric and ionospheric processes from off-electrojet low latitude presented in the previous section can be summarized as follows:

1. Mesospheric and E region echoes observed during daytime are found to occur mostly in the height ranges of 65–77 km and 87–102 km, respectively. While there is no specific local time preference for the mesospheric echoes to occur, the E region echoes in the equinoxes occur mostly in the forenoon. Both mesospheric and E region echoes display layered morphology with descending pattern reminiscent of tidal/gravity wave characteristics.

2. While the seasonal variations of mesospheric echo occurrence show semiannual variation with their maxima in the equinoxes, the seasonal variations of the E region echo occurrence show strong annual variation peaking in the summer and two secondary maxima identical to semiannual variation of the mesospheric echoes. The occurrence rates of the E region echoes also show year-to-year variability.

3. Seasonal variations of temperature, obtained from SABER observations, show mesopause (coldest temperature) occurring around 98 km with secondary minima occurring around 75 km. The secondary minima, accompanied with temperature inversion, show semiannual variations with peaks during the equinoxes and display descending pattern with a descent rate of 1 km/month.

4. Seasonal variations of wind and wind shear observed in the lower mesosphere (65–80 km) show semiannual variations with peaks occurring during the equinoxes. Zonal wind in the upper mesosphere (80–98 km) is characterized by wind shear with descending phase consistent with tidal behavior and shows large seasonal variations with distinctly different behavior in the summer.

5. Tidal activities (both diurnal and semidiurnal) are found to be maximum in the equinoxes and summer, and the enhanced amplitude of the diurnal tide in the zonal wind in the summer is found to be linked with nonmigrating tide.

6. Seasonal variations of gravity wave associated kinetic energy show semiannual variations with maxima occurring in the equinoxes.

7. Seasonal variations of meteor count (a proxy of metallic ions) show conspicuous maxima in the summer, secondary maxima in the winter, and minimum in the equinoxes.

8. Seasonal variations of the mesospheric echo occurrence as well as the height variation of the echoing region are well corroborated with the negative temperature gradients associated with the secondary temperature minima. Seasonal variations of the mesospheric echo occurrence are also well correlated with large wind shear, tidal, and gravity wave activity in the equinoxes.

9. Seasonal variations of the E region echo occurrence are well correlated with E_s activity, zonal wind and wind shear, and tidal activities. The E region echo occurrence, however, is not simply correlated with those of meteor count except for the summer when both show maximum activity.

10. The morphology of the E region echoes and their descending behavior are closely linked with those of E_s and vertical shear in zonal wind. Descending layer morphology of the mesospheric echoes in a few case studies is also found to be consistent with tidal behavior.

Results presented above clearly suggest that semiannual variations, with equinoctial maxima, in the occurrence of low-latitude mesospheric echoes are closely linked with similar variations in the occurrences of temperature inversion, large wind shear, tidal, and gravity wave activities in the same height region. For the E region echoes, the summer maximum and equinoctial secondary maxima are found to be linked with similar variations in wind and wind shear, E_s activity, tidal, and gravity wave activities. In addition, the summer maximum in the E_s and E region FAI is closely correlated with meteor flux and nonmigrating diurnal tide. This finding is significant given the fact that such wind field in the presence of metallic ions could form both E_s and FAI. It may, however, be mentioned that the occurrence rates of the E region echoes also varied from 1 year to the other and hence the aforementioned results have to be further verified using a larger database than that used here.

Semiannual and annual variations in various background parameters reported here are consistent with the semiannual and annual oscillations reported earlier from various low-latitude stations [e.g., *Takahashi et al.*, 1995; *Garcia et al.*, 1997; *Siva kumar et al.*, 2001; *Taylor et al.*, 2005; *Guharay et al.*, 2009]. The seasonal variations in the tidal and gravity wave activities are also consistent with those reported earlier [e.g., *Reddi and*

Ramkumar, 1997; *Sridharan and Sathishkumar*, 2008; *Venkateswara Rao et al.*, 2008, 2012]. However, it is important to mention that the gravity wave periods considered by *Sridharan and Sathishkumar* [2008] were 2–6 h and the gravity wave variances reported by them peaked in the equinoxes. Also, *Venkateswara Rao et al.* [2008] dealt with short-period gravity wave activity (<30 min) based on observations of *E* region quasi-periodic echoes and found that the gravity wave activity was maximum during the summer, followed by equinoxes and winter.

Having found that seasonal variations in the potential free energy sources, such as temperature gradient and wind shear in the mesosphere, metal ion rich E_s layer providing electron density gradient, and wind, agree extremely well with the observed seasonalities of the mesospheric and *E* region echo occurrences, it is also found that tidal and gravity wave activities are the important drivers for the observed seasonality.

Although we have not investigated the causes for the seasonality of the gravity wave activity during 2011–2012, the observed equinoctial maxima in the gravity wave activity can be attributed to selective filtering of gravity waves by the stratospheric and mesospheric wind field (associated with SAO and QBO) [*Dunkerton*, 1982]. This being the case, it is important to understand the coupling of tides and gravity waves with the background and their mutual coupling.

Occurrence of large westward wind and wind shear around the mesospheric echoing region can be attributed to selective absorption of upward propagating gravity waves in the background flow due to critical level interaction [*Fritts and Alexander*, 2003]. Those gravity waves which break/dissipate due to either convective or dynamical instability result in turbulence and heat consistent with the mesospheric echoes and temperature inversion [*Sridharan et al.*, 2008]. There will still be some left out gravity waves, which would neither be absorbed in the background nor be unstable, which will propagate farther up and interact with the *E* region wind modifying the E_s layers formed by tidal winds and manifest as *E* region FAI. Apart from gravity waves, migrating diurnal tides in the mesosphere and lower thermosphere region also provide large westward acceleration. *Lieberman and Hays* [1994] reported the acceleration of the zonal mean flow induced by tides in the equatorial lower thermosphere. Later, *McLandress et al.* [2006] also reported that the migrating diurnal tide provides most of the westward wave forcing in the equatorial upper mesosphere.

The gravity waves can also interact with the tides. Earlier investigations have also shown that gravity waves can interact with both diurnal and semidiurnal tides [*Thayaparan et al.*, 1995; *Liu et al.*, 2000; *Sridharan et al.*, 2008] manifesting temperature and wind structures in the mesosphere and lower thermosphere. *Sridharan et al.* [2008] using low-latitude observations over the Indian region showed that interaction of gravity wave and diurnal tide was responsible for mesospheric temperature inversion. We have also found that the temperature inversion layer descends with 1 km/h consistent with that expected from numerical simulation of gravity wave and tidal interaction [*Liu et al.*, 2000]. Given the fact that temperature inversions are accompanied by cooling at both below and above the warming region, it is also quite likely that the heating is due to gravity wave breaking. It is also known that the momentum deposited by gravity waves modulates both amplitude and phase of tides and also shorten their vertical wavelengths [*Fritts and Vincent*, 1987]. In the present study, we have also observed that the vertical wavelength of the diurnal tide in zonal wind is of the order of 7 km during the month of June and July, which may be attributed to gravity wave-tide interactions. Further, gravity wave propagation and dissipation can be modulated by tidal oscillations. Thus, the interaction between gravity waves and tides may influence the MLT region background thermal and wind structures leading to the mesospheric echoes through turbulence generation. In fact, similar seasonal variations in gravity wave variance and turbulent kinetic energy dissipation rate [*Selvaraj et al.*, 2016] indicate the role of gravity wave breaking in generating turbulence and heat responsible for the mesospheric temperature inversion. *Liu et al.* [2000], through numerical simulation, also showed that the heating could be large enough to cause inversion.

With regard to the *E* region echoes, we find that tidal wind plays the most important role in the seasonal evolution of *E* region echo occurrence. In particular, for the annual variation in the *E* region echo occurrence (in the summer), we have shown the roles of diurnal tidal wind having short vertical wavelength (presumably nonmigrating in nature), gravity wave, and metallic ions. In addition to this, we have also shown that in the summer zonal wind at lower altitudes is strongly eastward, which itself can make the *E* layer unstable. We also surmise that the intensification of E_s layer and FAI occurrence during the summer is partly due to the interaction of gravity wave and diurnal tidal wind having short vertical wavelength (nonmigrating

nature). This is consistent with the large occurrence rate of quasiperiodic echoes during the summer [*Venkateswara Rao et al.*, 2008]. Due to slow downward phase progression of such short wavelength diurnal tide, E_s layer formed by such wind also moved downward slowly and the gravity waves have enough time to modulate the E_s layer forming structures, which become unstable by the gradient drift instability. In the equinoxes, the secondary maxima in the FAI occurrence are presumably linked with semiannual variations in tidal and gravity wave associated winds. During the equinox, however, the diurnal tide has vertical wavelength of 20–25 km and hence the tidal node moves rather fast and come to collision-dominated lower E region, consistent with low occurrence rate in the afternoon.

With regard to the meteor flux, while we find that the seasonal variations of meteor flux show a conspicuous maximum in the summer, consistent with the summer maximum of the E_s and E region echoes, the secondary maxima in the E region echo occurrence is consistent with the seasonal variation of E_s but not consistent with that of meteor flux. Similar inconsistency can be noted for the winter when meteor flux is considerably high, but E_s and E region echoes have low occurrence. Apparently, the seasonal variations of meteor flux appear to be inconsistent with the seasonal variations of E_s and E region FAI and are different from that reported from midlatitude [*Haldoupis et al.*, 2007]. It may be mentioned that *Haldoupis et al.* [2007] found excellent correlation between the seasonal variation of meteor flux and E_s. The role of meteor flux on the low-latitude E_s and FAI needs further investigation.

References

Belova, E., S. Kirkwood, T. Narayana Rao, S. Satheesh Kumar, and T. Sergienko (2012), Spectral characteristics and scatter cross-section of low latitude mesospheric echoes measured by the Indian MST radar at Gadanki, *Ann. Geophys.*, *30*, 983–990, doi:10.5194/angeo-30-983-2012.

Chandra, H., H. S. S. Sinha, U. Das, R. N. Misra, S. R. Das, J. Datta, S. C. Chakravarty, A. K. Patra, N. V. Rao, and D. N. Rao (2008), First mesospheric turbulence study using coordinated rocket and MST radar measurements over Indian low latitude region, *Ann. Geophys.*, *26*, 2725–2738, doi:10.5194/angeo-26-2725-2008.

Chau, J. L., R. F. Woodman, and L. A. Flores (2002), Statistical characteristics of low-latitude ionospheric field-aligned irregularities obtained with the Piura VHF radar, *Ann. Geophys.*, *20*, 1203–1212, doi:10.5194/angeo-20-1203-2002.

Dunkerton, T. J. (1982), Theory of the mesopause semiannual oscillation, *J. Atmos. Sci.*, *39*, 2681–2690.

Fritts, D. C., and M. J. Alexander (2003), Gravity wave dynamics and effects in the middle atmosphere, *Rev. Geophys.*, *41*(1), 1003, doi:10.1029/2001RG000106.

Fritts, D. C., and R. A. Vincent (1987), Mesospheric momentum flux studies at Adelaide, Australia: Observations and a gravity wave–tidal interaction model, *J. Atmos. Sci.*, *44*(3), 605–619, doi:10.1175/1520-0469(1987)044<0605:MMFSAA>2.0.CO;2.

Garcia, R. R., T. J. Dunkerton, R. S. Lieberman, and R. A. Vincent (1997), Climatology of the semiannual oscillation of the tropical middle atmosphere, *J. Geophys. Res.*, *102*, 26,019–26,032, doi:10.1029/97JD00207.

Guharay, A., D. Nath, P. Pant, B. Pande, J. M. Russell III, and K. Pandey (2009), Observation of semiannual and annual oscillation in equatorial middle atmospheric long term temperature pattern, *Ann. Geophys.*, *27*, 4273–4280.

Hedin, A. E. (1991), Extension of the MSIS thermosphere model into the middle and lower atmosphere, *J. Geophys. Res.*, *96*, 1159–1172.

Haldoupis, C., D. Pancheva, W. Singer, C. Meek, and J. MacDougall (2007), An explanation for the seasonal dependence of midlatitude sporadic E layers, *J. Geophys. Res.*, *112*, A06315, doi:10.1029/2007JA012322.

Kumar, K. K., G. Ramkumar, and S. T. Shelbi (2007a), Initial results from SKiYMET meteor radar at Thumba (8.5°N, 77°E): 1. Comparison of wind measurements with MF spaced antenna radar system, *Radio Sci.*, *42*, RS6008, doi:10.1029/2006RS003551.

Kumar, G. K., M. V. Ratnam, A. K. Patra, V. V. M. J. Rao, S. V. B. Rao, and D. N. Rao (2007b), Climatology of low latitude mesospheric echo characteristics observed by Indian mesosphere, stratosphere, and troposphere radar, *J. Geophys. Res.*, *112*, D06109, doi:10.1029/2006JD007609.

Lehmacher, G. A., L. Guo, E. Kudeki, and J. Chau (2007), High resolution observations of mesospheric layers with the Jicamarca VHF radar, *J. Adv. Space Res.*, *40*, 734–743, doi:10.1016/j.asr.2007.05.059.

Lieberman, R. S., and P. B. Hays (1994), An estimate of the momentum deposition in the lower thermosphere by the observed diurnal tide, *J. Atmos. Sci.*, *51*, 3094–3105, doi:10.1175/1520-0469(1994)051<3094:AEOTMD>2.0.CO;2.

Liu, H.-L., M. E. Hagan, and R. G. Roble (2000), Local mean state changes due to gravity wave breaking modulated by the diurnal tide, *J. Geophys. Res.*, *105*, 12,381–12,396, doi:10.1029/1999JD901163.

McLandress, C., W. E. Ward, V. I. Fomichev, K. Semeniuk, S. R. Beagley, N. A. McFarlane, and T. G. Shepherd (2006), Large-scale dynamics of the mesosphere and lower thermosphere: An analysis using the extended Canadian Middle Atmosphere Model, *J. Geophys. Res.*, *111*, D17111, doi:10.1029/2005JD006776.

Patra, A. K., S. Sripathi, V. Sivakumar, and P. B. Rao (2004), Statistical characteristics of VHF radar observations of low latitude E region irregularities over Gadanki, *J. Atmos. Sol. Terr. Phys.*, *66*, 1615–1626, doi:10.1016/j.jastp.2004.07.032.

Patra, A. K., S. Sripathi, P. B. Rao, and R. K. Choudhary (2006), Gadanki radar observations of daytime E region echoes and structures extending down to 87 km, *Ann. Geophys.*, *24*, 1–9, doi:10.5194/angeo-24-1861-2006.

Patra, A. K., N. Venkateswara Rao, D. V. Phanikumar, H. Chandra, U. Das, H. S. S. Sinha, T. K. Pant, and S. Sripathi (2009), A study on the low-latitude daytime E region plasma irregularities using coordinated VHF radar, rocket-borne, and ionosonde observations, *J. Geophys. Res.*, *114*, A11301, doi:10.1029/2009JA014501.

Patra, A. K., P. P. Chaitanya, and A. Bhattacharyya (2012), On the nature of radar backscatter and 250 MHz scintillation linked with an intense daytime Es patch, *J. Geophys. Res.*, *117*, A03315, doi:10.1029/2011JA016981.

Rajaram, R., and S. Gurubaran (1998), Seasonal variations of low-latitude mesospheric winds, *Ann. Geophys.*, *16*, 197–204, doi:10.1007/s00585-998-0197-4.

Rao, P. B., A. R. Jain, P. Kishore, P. Balamuralidhar, S. H. Damle, and G. Viswanathan (1995), Indian MST Radar: I. System description and sample vector wind measurements in ST mode, *Radio Sci.*, *30*, 1125–1138, doi:10.1029/95RS00787.

Reddi, C. R., and G. Ramkumar (1997), Climatologies of tidal winds in the radio-meteor region over Trivandrum (8°N), *J. Atmos. Sol. Terr. Phys.*, *59*, 1757–1777.

Royrvik, O. (1983), VHF radar signals scattered from the equatorial mesosphere, *Radio Sci.*, *18*, 1325–1335, doi:10.1029/RS018i006p01325.

Royrvik, O., and L. G. Smith (1984), Comparison of mesospheric VHF radar echoes and rocket probe electron concentration measurements, *J. Geophys. Res.*, *89*, 9014–9022, doi:10.1029/JA089iA10p09014.

Sasi, M. N., and L. Vijayan (2001), Turbulence characteristics in the tropical mesosphere as obtained by MST radar at Gadanki (13.5°N, 79.2°E), *Ann. Geophys.*, *19*, 1019–1025, doi:10.5194/angeo-19-1019-2001.

Selvaraj, D., A. K. Patra, and D. Narayana Rao (2016), On the seasonal variations of reflectivity and turbulence characteristics of low-latitude mesospheric echoes over Gadanki, *J. Geophys. Res. Atmos.*, *121*, 6164–6177, doi:10.1002/2015JD024283.

Sheth, R. E., E. Kudeki, G. Lehmacher, M. Sarango, R. F. Woodman, J. Chau, L. Guo, and P. Reyes (2006), A high-resolution study of mesospheric fine structure with the Jicamarca MST radar, *Ann. Geophys.*, *24*, 1281–1293, doi:10.5194/angeo-24-1281-2006.

Siva kumar, V., Y. Bhavani Kumar, K. Raghunath, P. B. Rao, M. Krishnaiah, K. Mizutani, T. Aoki, M. Yasui, and T. Itabe (2001), Lidar measurements of mesospheric temperature inversion at a low latitude, *Ann. Geophys.*, *19*, 1039–1044, doi:10.5194/angeo-19-1039-2001.

Sridharan, S., and M. Sandhya (2014), E region radar echoes from low-latitude field-aligned irregularities due to gravity waves and tides: A case study using radar, lidar, and radiosonde observations and simulations, *J. Geophys. Res. Space Physics.*, *119*, 3094–3105, doi:10.1002/2013JA019273.

Sridharan, S., and S. Sathishkumar (2008), Seasonal and interannual variations of gravity wave activity in the low-latitude mesosphere and lower thermosphere over Tirunelveli (8.7°N, 77.8°E), *Ann. Geophys.*, *26*, 3215–3223, doi:10.5194/angeo-26-3215-2008.

Sridharan, S., S. Sathishkumar, and S. Gurubaran (2008), Influence of gravity waves and tides on mesospheric temperature inversion layers: Simultaneous Rayleigh lidar and MF radar observations, *Ann. Geophys.*, *26*, 3731–3739, doi:10.5194/angeo-26-3731-2008.

Takahashi, H., B. R. Clemesha, and P. P. Batista (1995), Predominant semi-annual oscillation of the upper mesospheric airglow intensities and temperatures in the equatorial region, *J. Atmos. Terr. Phys.*, *57*, 407–414.

Taylor, M. J., A. K. Taori, D. R. Hatch, H. L. Liu, and R. G. Roble (2005), Characterization of the semi-annual oscillation in mesospheric temperatures at low-latitudes, *Adv. Space Res.*, *35*, 2037–2043, doi:10.1016/j.asr.2005.05.111.

Thayaparan, T., W. K. Hocking, and J. MacDougall (1995), Observational evidence of gravity wave-tidal interactions using UWO 2 MHz radar, *Geophys. Res. Lett*, *22*, 381–384, doi:10.1029/94GL03270.

Venkateswara Rao, N., A. K. Patra, T. K. Pant, and S. V. B. Rao (2008), Morphology and seasonal characteristics of low latitude E-region quasiperiodic echoes studied using large database of Gadanki radar observations, *J. Geophys. Res.*, *113*, A07312, doi:10.1029/2007JA012830.

Venkateswara Rao, N., T. Tsuda, and Y. Kawatani (2012), A remarkable correlation between short period gravity waves and semiannual oscillation of the zonal wind in the equatorial mesopause region, *Ann. Geophys.*, *30*, 703–710.

Woodman, R. F., and A. Guillen (1974), Radar observations of winds and turbulence in the stratosphere and mesosphere, *J. Atmos. Sci.*, *31*, 493–505, doi:10.1175/1520-0469(1974)031<0493:ROOWAT>2.0.CO;2.